

Confinement Reinforcement for Under-Reinforced Ultrahigh-Performance Concrete Beams under Flexure

Cancan Yang* (corresponding author) – Ph.D. Candidate, 206 Ketter Hall, Department of Civil, Structural and Environmental Engineering, Buffalo, NY 14260 USA, Phone: 716-464-0639, Email: cancanya@buffalo.edu

Ankit Bhargava – Graduate Student, Department of Civil, Structural and Environmental Engineering, Buffalo, NY 14260 USA, Phone: 716-431-0092, Email: ab254@buffalo.edu

Mayur Bhuralal Purohit – Graduate Student, Department of Civil, Structural and Environmental Engineering, Buffalo, NY 14260 USA, Phone: 716-816-5566, Email: mayurbhu@buffalo.edu

Pinar Okumus, Ph.D. – Assistant Professor, 222 Ketter Hall, Department of Civil, Structural and Environmental Engineering, Buffalo, NY 14260 USA, Phone: 716-645-4356, Email: pinaroku@buffalo.edu

Abstract

Ultrahigh-performance Concrete (UHPC) flexural members with high compression strengths need large amounts of steel confinement to meet the current code confinement requirements. This study investigated the impact of different steel confinement amounts on the flexural behavior of longitudinally reinforced UHPC beams. Four small beam specimens with different steel confinement reinforcement amounts and grades were tested under monotonic three-point loading until failure. Steel confinement reinforcement grades varied from Grade 60 to Grade 120. The confinement volumetric ratios of the four specimens were 50%, 110%, 30%, and 50% of the minimum requirement of ACI 318-14. All specimens were under-reinforced longitudinally. The specimen with the least amount of confinement failed due to excessive shear cracking. The other specimens failed under flexure in the form of longitudinal reinforcement fracture, and exhibited similar flexural strength and ductility levels regardless of the confinement amount. These results indicated the need for re-evaluating ACI 318-14 requirements on the confinement for UHPC flexural members, especially when the longitudinal reinforcement ratios are low.

A numerical analysis based on section equilibrium was conducted and evaluated using the test results. The constitutive tensile model of UHPC was obtained through material tests. Several unconfined and confined concrete compression models in the literature were examined. Compared to the compression models developed for normal concrete, the existing models for fiber-reinforced high-strength concrete significantly improved the predictions of flexural moment strength and failure mode for UHPC.

Keywords: Ultrahigh-performance concrete; Fiber reinforced concrete; High strength concrete; Flexure, High-strength steel; Confinement; Ductility; Constitutive model.

1. Introduction

Ultra-high performance concrete (UHPC) has been investigated to enhance damage tolerance, dissipate energy, or reduce residual deformations (Billington and Yoon 2004; Yang and Okumus 2017). Zhang et al. (2013), Fischer and Li (2003), and Osorio et al. (2014) demonstrated that fiber-reinforced concrete improved ductility, allowing a reduction in confinement reinforcement area. However, these studies were limited to concrete strengths lower than 12 ksi (82.7 MPa).

The efficiency of confinement decreases for higher strengths of concrete, which have lower dilation tendencies (Paultre et al. 2001). High strength flexural members that are not well confined may experience brittle failures. Additional confinement reinforcement can be added to overcome this issue. Similarly, discontinuous fibers added to concrete may increase ductility. However, knowledge on the confined properties of high strength, fiber reinforced concretes is limited. This paper investigated the effect of confinement reinforcement on high strength, fiber reinforced concrete and evaluated the confinement requirements of codes for such concrete types through testing, moment-curvature analyses and finite element analyses.

Following the code requirements for confinement reinforcement may results in an impractical amount of reinforcement for UHPC. Therefore, in addition to studying 60 ksi (413.7 MPa) yield strength confinement reinforcement, high-yield strength steel (HSS) (yield strengths larger than 80 ksi (550 MPa)) reinforcement was also included in the study. Previous uniaxial compression tests have shown that HSS as transverse reinforcement can improve post-peak and compressive ductility of high-strength concrete (Hosinieh et al. 2015). Table 1 summarizes the literature on the flexural behavior of high-strength fiber reinforced concrete, reinforced with normal-strength steel (NSS) and HSS as transverse reinforcement. However, a direct comparison of behavior of high-strength concrete confined with NSS and HSS for the same concrete strength and volumetric ratio is missing from the literature. This research fills this gap.

Table 1. Literature on fiber reinforced concrete with high-strength steel under flexure (1 ksi = 6.9 MPa)

| Ref. | Concrete type | Confinement | | Failure mode | Major conclusions |
|--------------------------|--|--------------|----------------|-------------------|--|
| | | Yield stress | Vol. Ratio | | |
| (Kawashima et al. 2011) | ¹ NC, 8.7ksi ¹ SFRC, 8.7ksi) ¹ PFRC, 5.8ksi | 50ksi | 1.7% | Reinf. rupture | Mitigating damage to concrete cover and core: ¹ PFRC> ¹ SFRC> ¹ NC; ¹ NC, ¹ SRFC, ¹ PFRC exhibit similar flexural strength and ductility capacity. |
| (Ibarra and Bishaw 2016) | ¹ HSC, 15.8-19.0ksi ¹ HSFRC, 13.5-15.3ksi | 60 or 100ksi | 1.48% or 0.87% | Reinf. rupture | Compared to NSS, ² UHSS increased flexural capacity by more than 60%, but decreased ductility by 40%. The addition of steel fibers did not improve ductility. |
| (Paultre et al. 2001) | ¹ HSC, 11.6-17.4ksi | 61-120ksi | 1.96% - 4.26% | Concrete crushing | ² HYSS can successfully decrease the amount of transverse reinforcement. |
| (Sugano et al. 2007) | ¹ UFC, 29ksi | 190ksi | 0.53% - 2.29% | Concrete crushing | Stable seismic behavior of columns can be obtained under very high lateral reinforcements. |

¹NC: normal concrete; SFRC: steel fiber reinforced concrete; PFRC: polypropylene fiber reinforced concrete; HSC: high-strength concrete; HSFRC: high-strength steel fiber-reinforced concrete; HPFRC: high-performance fiber-reinforced concrete
UFC: ultra-high-strength fiber-reinforced concrete.

²UHSS: ultra-high-strength steel; HYSS: high-yield-strength steel.

Several confinement models were recently established for high-strength reinforced concrete with and without fibers (Hosinih et al. 2015; Legeron and Paultre 2003; Razvi and Saatcioglu 1999; Sugano et al. 2007). These confinement models were developed based on uniaxial compression tests on reinforced concrete columns. In this study, the confinement model developed by Sugano et al. (2007) was used in the numerical analysis because this model considers both steel fiber reinforced high-strength concrete and HSS confinement. This study investigated the impact of different steel confinement amounts on the flexural behavior of longitudinally reinforced UHPC beams. Four beam specimens with different steel confinement amounts and grades were tested under monotonic three-point loading until failure. Specimens included ones that meet and do not meet code requirements for confinement reinforcement. Numerical analyses that were built on section equilibrium were conducted with the objective of evaluating the applicability of different unconfined and confined concrete compression models to UHPC.

2. Experimental Investigation

2.1 Specimens and Experimental Set-up

Four small UHPC beam specimens were tested. Their dimensions, cross sections, and mild steel reinforcement layouts are provided in Figure 1. The concrete cover was 0.5 in (12.7 mm). UHPC used in all the specimens had the Ductal[®] light grey premix of LafargeHolcim (Lafarge Canada Inc. 2018). PVA (polyvinyl alcohol) fibers with the volumetric ratio of 2% were used. The PVA fibers were 0.008 in. (0.2 mm) in diameter and 0.5 in. (12.7 mm) in length. Although materials for the mix were provided by LafargeHolcim, the mix was developed for this study and is not a commercial Ductal[®] product. Measured compressive strength of the mix varied between 15.8 and 17.4 ksi (108.9 and 120.0 MPa), lower than some of the commonly used commercial Ductal[®] mixes (e.g., compressive strengths of Ductal[®] JS1000 and Ductal[®] AN1000 are 20 ksi (150 MPa) and 17 ksi (120 MPa), respectively). Lower compression strength is a result of differences in proportions of the mix used in this study and commercial mixes, including the smaller premix-to-water ratio. The longitudinal reinforcement ratios for all specimens were 1.5%.

The difference between the specimens was the steel confinement amounts and grades, as summarized in Table 2. The ratio of the transverse reinforcement volumetric ratio provided ($\rho_{L_provided}$) versus the minimum requirement per ACI 318 (2014) ($\rho_{L_required}$) was calculated. Only Specimen 2 met the code requirement. The confinement volumetric ratios provided were 50%, 30%, and 50% of the required amount for Specimens 1, 3 and 4, respectively. Grade 60 and Grade 120 confinement reinforcement were specified per ASTM A615 (2018) and ASTM A1035 (2016), respectively.

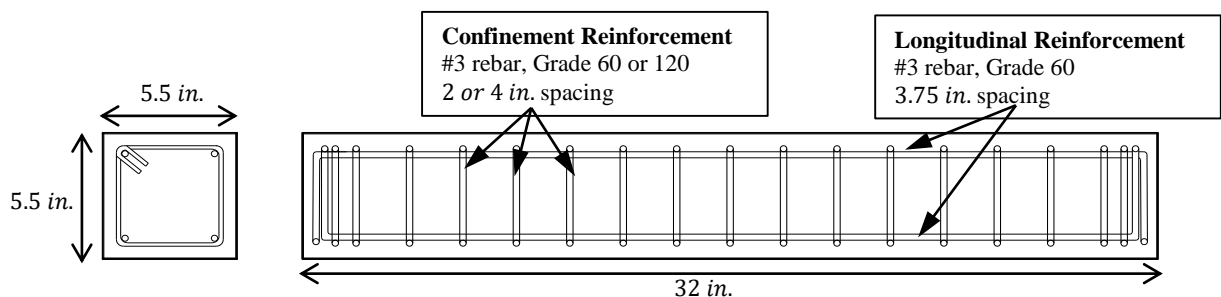


Figure 1. Beam Specimen Details (1 in. = 25.4 mm)

Table 2. Confinement Reinforcement for the Specimens

| Specimen | Confinement steel grade | Confinement spacing | $\rho_{l_provided}/\rho_{l_required}$ |
|----------|-------------------------|---------------------|---|
| 1 | Grade 60 | 2 in. (50.8 mm) | 0.5 |
| 2 | Grade 120 | 2 in. (50.8 mm) | 1.1 |
| 3 | Grade 60 | 4 in. (101.6 mm) | 0.3 |
| 4 | Grade 120 | 4 in. (101.6 mm) | 0.5 |

The experimental set-up is shown in Figure 2. Monotonic three-point loading was quasi-statically applied through an MTS Axial-Torsion Universal testing machine (MTS Systems Corporation, Eden Prairie, MN, USA). The MTS machine is capable of applying ± 100 kips (± 444.8 kN) with a 10-in. (254-mm) stroke. The displacement-controlled loading was applied with a constant rate of 0.01 in./min. (0.254 mm/min.) until failure. The curvature was calculated at different locations (at mid-span, and at 2-in. (50.8-mm) to the left and at 2-in. (50.8-mm) to the right of the mid-span) from longitudinal strains and displacements measured using six linear potentiometers. The mid-span displacement and applied force were measured by the displacement sensor and load cell in the MTS testing machine, respectively.

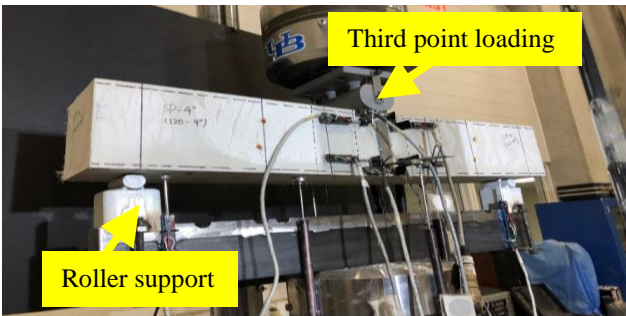
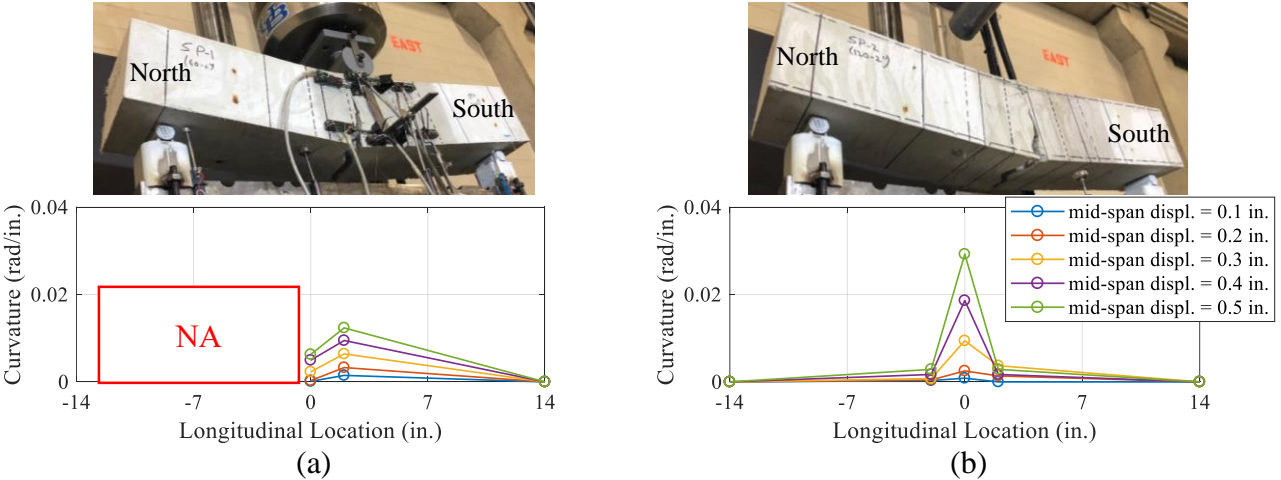


Figure 2. Experimental set-up

3. Test Results

Figure 3 shows specimens at the end of the tests, and the curvature distributions along the length for all specimens. For Specimen 1, the curvature at 2-in. (50.8 mm) from the middle span is not shown due to the malfunction of the linear potentiometer.



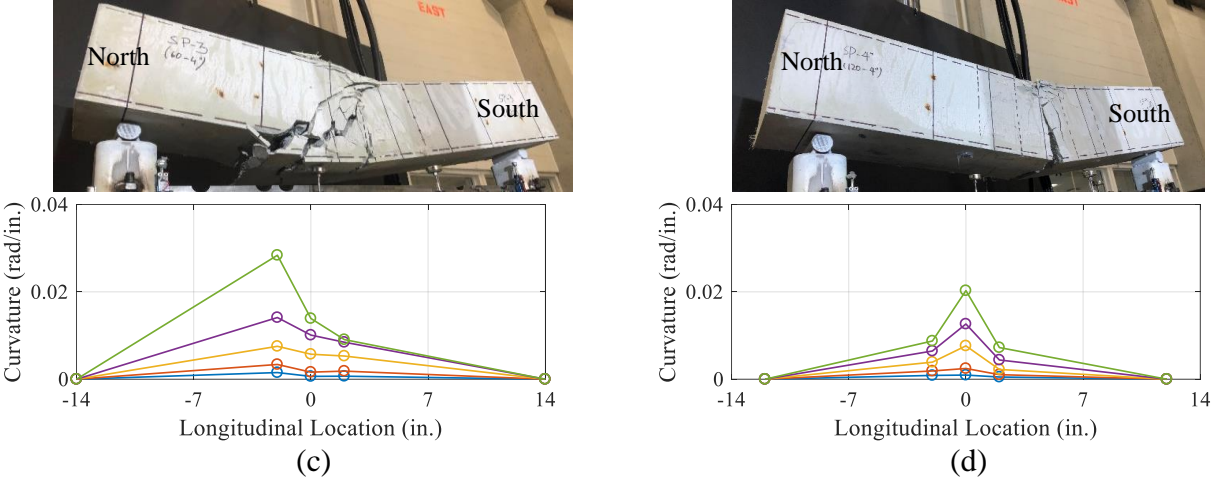


Figure 3. Damage pattern and curvature distribution along the length of the beam for (a) Specimen 1, (b) Specimen 2, (c) Specimen 3, and (d) Specimen 4 (1 in. = 25.4 mm)

Specimen 1, 2 and 4 failed under flexure. For these specimens, multiple cracks formed before the peak load was reached. After the peak moment, the width of a single crack increased significantly compared to the other cracks. Fibers started to pull out and the deformation of the longitudinal rebar was localized at this specific crack location. The localized crack opening was at the mid-span for Specimen 2 and 4, and at about 2-in. (50.8 mm) to the north of the mid-span for Specimen 1. Unlike Specimens 1,2 and 4, Specimen 3 failed due to excessive shear cracking. This might be due to the larger spacing and lower grade of the transverse reinforcement in this specimen.

Figure 4 shows the measured moment-midspan displacement relationships for all four specimens. For Specimen 1, 2 and 4, a significant moment drop occurred once the longitudinal steel rebar ruptured across the widest crack. Since Specimen 3 failed due to shear, the measured moment degraded rapidly once the inclined crack opening became significant.

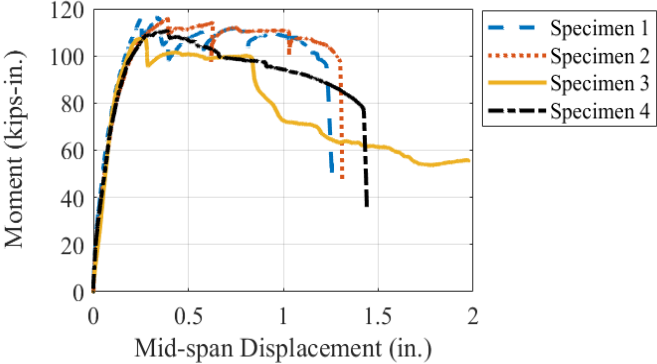


Figure 4. Moment-midspan displacement relationships of reinforced UHPC beams (1 kip = 4.4 kN, 1 in. = 25.4 mm)

Specimen 3 had a smaller displacement ductility due to the shear failure mode. Specimen 1 and 2 had similar displacement ductility levels. Multiple drops in moment were due to the widening of a single localized crack, followed by an increase in moment that is caused by fiber bridging. Specimen 4 did not maintain its moment strength as well as specimens 1 and 2 did, after reaching its peak strength. The confinement volumetric ratio provided for Specimen 1 and 4 were

only 50% of the minimum required by ACI 318 (2014). However, they were shown to have similar displacement ductility levels as Specimen 2 (the only specimen that meets the code requirement). This indicates that the ACI 318 (2014) confinement requirements may be too conservative and needs to be re-evaluated for UHPC flexural members.

4. Numerical Investigation

This section examines the applicability of using different unconfined and confined concrete compression models to predict the flexural response of the beam specimens tested.

4.1. Material Constitutive Model

4.1.1. UHPC

4.1.1.1. Compression

The elastic modulus of UHPC was calculated per Graybeal (2006). Two sets of compression models were used to define the compressive behavior of UHPC, referred to as case 1 and case 2 as shown in Table 3. In case 1, material models developed and widely used for conventional concrete were used after they were adjusted for strength. These compression stress-strain models were developed by Popovics (1973) and Mander et al. (1988) for unconfined and confined concrete, respectively.

In case 2, material models developed specifically for fiber reinforced concrete were used. The existing compression models for PVA fiber reinforced concrete are mostly developed for concrete with compression strengths lower than 12 ksi (82.7 MPa) (Han et al. 2003; Xu and Cai 2010; Zhou et al. 2014). Due to this limitation, the compressive behavior of unconfined UHPC was defined following Hosinieh et al. (2015) for 2% steel fiber reinforced high-strength concrete. This model covers compression strengths up to 20 ksi (137.9 MPa). The stress-strain relationship of confined UHPC was calculated as per Sugano et al. (2007). This confinement model was selected because this model considers both steel fiber reinforced high-strength concrete and HSS confinement.

Table 3. Compressive constitutive models for unconfined and confined UHPC

| Case No. | Unconfined UHPC | Confined UHPC |
|----------|------------------------|----------------------|
| 1 | (Popovics 1973) | (Mander et al. 1988) |
| 2 | (Hosinieh et al. 2015) | (Sugano et al. 2007) |

The compression stress-strain curves developed using case 1 and case 2 are plotted in Figure 5. Both cases were used to calculate the flexural response of the beam specimens. Compression tests were carried out per ASTM C109/C109M (2016) with 2-in. (50.8 mm) cube specimens. Compression test results of four cube specimens are also shown in Figure 5 as a comparison. The measured elastic modulus was smaller than the one calculated per Graybeal (2006). The compressive behavior of UHPC in the post-peak strength range was underestimated by both case 1 and case 2 unconfined compression models.

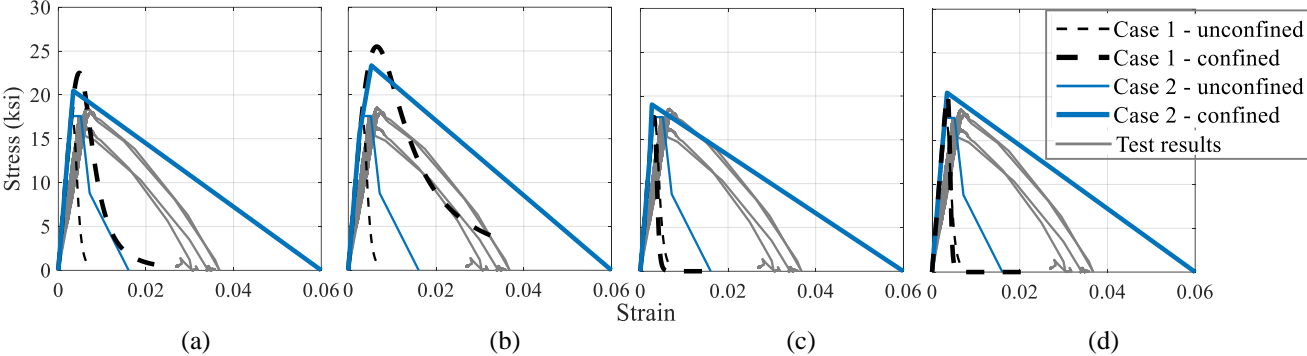


Figure 5. Compressive stress-strain relationships of unconfined and confined UHPC for (a) Specimen 1, (b) Specimen 2, (c) Specimen 3, and (d) Specimen 4, as tested and as predicted (1 ksi = 6.9 MPa)

4.1.1.2. Tension

In order to obtain nonlinear tensile properties of UHPC, a four-point flexure test was conducted on a beam made of UHPC without any mild reinforcement bars. This beam had the same dimensions as the other specimens with reinforcing. The measured moment-midspan displacement for this unreinforced UHPC beam is shown in Figure 6.

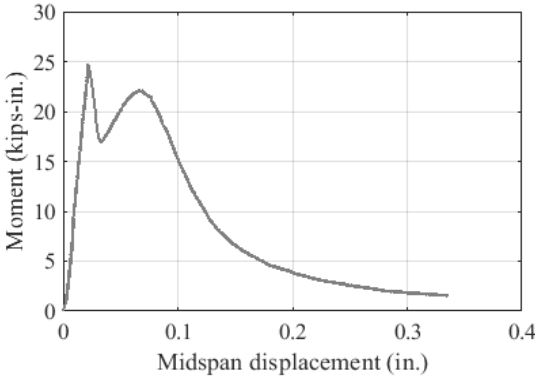


Figure 6. Measured moment-midspan displacement relationship for the unreinforced UHPC beam (1 kip = 4.4 kN, 1 in. = 25.4 mm)

The tensile strength was calculated as 0.64 ksi (4.4 MPa) using the measured moment at the end of the elastic range. The nonlinear tensile stress-strain relationship of UHPC, shown in Figure 7, was derived from the measured flexural response of this unreinforced beam shown in Figure 6 by varying tensile stress-strain relationship until a match is achieved between calculated and tested moment-displacement relationships. Figure 8 shows the calculated moment-curvature response for the unreinforced UHPC beam.

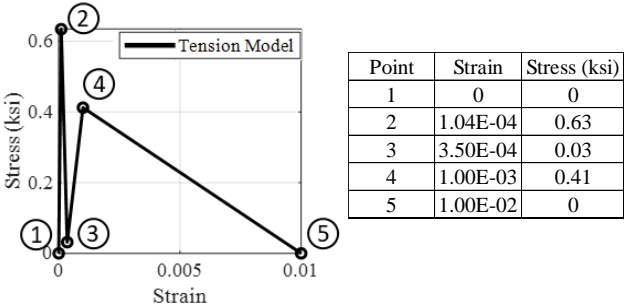


Figure 7. Calculated material constitutive model of UHPC for tension (1 ksi = 6.9 MPa)

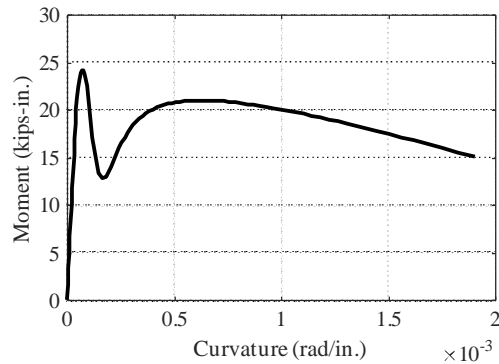


Figure 8. Calculated moment-curvature response of the unreinforced UHPC beam (1 kip = 4.4 kN, 1 in. = 25.4 mm)

4.1.2. Steel Rebar

The longitudinal reinforcement grade was Grade 60 with the minimum yield strength of 60 ksi (413.7 MPa) and the ultimate tensile strain of 0.09 (ASTM A615/A615M2 018). Figure 9 shows the stress-strain relationship measured from the tensile tests performed on longitudinal rebar coupons as well as the one calculated as per Mander (1984). The tensile stress-strain constitutive model developed by Mander (1984) predicted the behavior well for the longitudinal reinforcement.

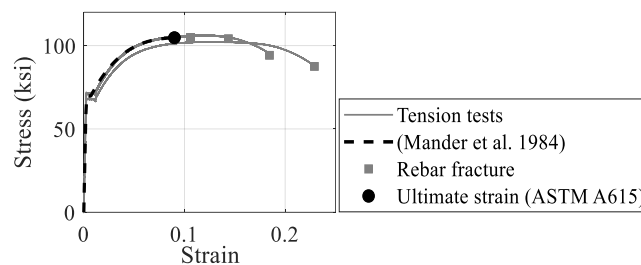


Figure 9. Mild steel rebar stress-strain relationship (1 ksi = 6.9 MPa)

4.2. Numerical Analytical Model

A monotonic moment-curvature analysis was performed for the tested beam specimens. The beam cross section was discretized into fibers categorized as confined or unconfined concrete (concrete cover). The neutral axis location, stresses and strains across the section were calculated from section equilibrium using the constitutive models described in section 4.1. Strain and stress distributions across the cross section were used to generate moment-curvature relationships by gradually increasing the compressive strain of the extreme fiber.

4.3. Numerical Analysis Results

Figure 10 shows the moment-curvature relationship calculated for the four tested beam specimens. The moment and curvature were calculated at mid-span, where they were the highest. The failure modes are shown with “x” or “o” as the reinforcement fracture and concrete crushing, respectively, on the figures. The measured curvatures of Specimen 1 and 3 were much smaller than the ones for Specimen 2 and 4, because the localized crack was not at mid-span for these specimens as shown in Figure 3. The measured moment-curvature relationships are available until the displacement reached 0.5 in. (12.7 mm).

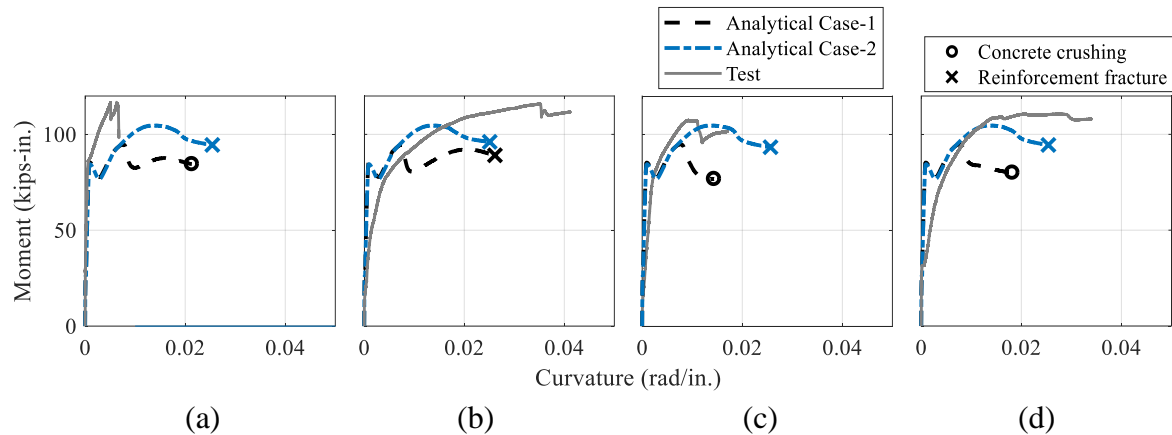


Figure 10. Comparison of moment-curvature relationships between test and analytical results for (a) Specimen 1, (b) Specimen 2, (c) Specimen 3, and (d) Specimen 4 (1 kip = 4.4 kN, 1 in. = 25.4 mm)

For all specimens, the first drop of moment in the analytical results occurred due to the first crack in concrete. The consequent increase in moment was due to fibers bridging cracks. For case 1, the second drop of moment in the analytical results was caused by cover concrete reaching the spalling strain limit. The peak moment strengths calculated analytically were consistently smaller than the ones obtained through test results for all specimens in case 1. For case 1, the analytical results correctly predicted the failure model of Specimen 2 as longitudinal reinforcement fracture, and incorrectly predicted the failure mode of the other specimens as concrete crushing.

The difference between the case 1 analytical model predictions and test results may be due to the under-prediction of concrete core crushing strain limit when the confinement model of Mander et al. (1988) was used for UHPC. With this model, the confinement potential of the fibers is not considered in the analysis.

Case 2 analyses predicted the maximum moment strength reasonably well. For all specimens, the differences between calculated and measured maximum moment strengths were less than 6%. The moment started decreasing after it reached the peak value because the cover concrete stress decreased at larger compressive strains, which led to the neutral axis shifting towards the tension side. The failure modes of all specimens (reinforcement fracture) except for Specimen 3 were correctly predicted by the analyses. The differences between the moment-curvature curves obtained from predictions and testing may be due to the assumption of linear strain distribution along the cross section height, particularly after crack opening.

The results indicated that using the compression models developed for normal concrete and adjusted for strength may result in an underestimation of peak flexural strength for all tested specimens and misprediction of flexural failure modes for Specimen 1, 3, and 4. However, the prediction results were improved using the existing compression models developed for fiber-reinforced high-strength concrete. Even though most material models for UHPC were developed for steel fiber reinforced concrete, these material models were better in predicting the behavior of PVA fiber reinforced concrete than the ones developed for normal concrete.

5. Summary and Conclusions

This study investigated the impact of different steel confinement amounts on the flexural behavior of longitudinally reinforced UHPC beams. The measured compressive strength of the UHPC mix used in this research varied between 15.8 and 17.4 ksi (108.9 and 120.0 MPa). The UHPC had

PVA fibers with a volumetric ratio of 2%. Four beam specimens with different steel confinement amounts and grades were tested under monotonic three-point loading until failure. Steel confinement reinforcement grades varied from Grade 60 to Grade 120. The longitudinal reinforcement ratios for all specimens were 1.5%. The specimen with the lower confinement steel grade and volumetric ratio failed due to excessive shear cracking. The other specimens failed under flexure in the form of longitudinal reinforcement fracture. Specimens with 50% and 100% confinement amount of the minimum requirement of ACI 318 (2014) exhibited similar flexural strength and ductility. This indicates that UHPC may not need the confinement reinforcement required by ACI 318 (2014). ACI 318 (2014) requirements on the confinement for UHPC flexural members should be re-evaluated, especially when the longitudinal reinforcement ratio is low.

Numerical analyses based on section equilibrium were conducted and were evaluated by comparing their results to test results. Constitutive compression relationship of UHPC was obtained through material tests. Constitutive tensile relationship of UHPC was derived from the compression models and modulus of rupture test data. The applicability of two sets of concrete compression models to UHPC was examined using the test results. The first set of compression models were developed for normal strength concrete. Using this set of compression models adjusting the concrete strength resulted in an underestimation of the peak flexural moment strength and misprediction of flexural failure modes. The prediction results were improved using the compression models developed for fiber-reinforced high-strength concrete.

6. References

Building Code Requirements for Structural Concrete and Commentary, ACI 318, American Concrete Institute, Farmington Hills, MI, 2014.

Standard Specification for Deformed and Plain, Low-Carbon, Chromium, Steel Bars for Concrete Reinforcement, ASTM A1035 / A1035M-16b, ASTM International, West Conshohocken, PA, 2016, www.astm.org.

Standard Specification for Deformed and Plain Carbon-Steel Bars for Concrete Reinforcement, ASTM A615 / A615M-18, ASTM International, West Conshohocken, PA, 2018 www.astm.org

Standard Test Method for Compressive Strength of Hydraulic Cement Mortars (Using 2-in. or [50-mm] Cube Specimens), ASTM C109 / C109M-16a, ASTM International, West Conshohocken, PA, 2016, www.astm.org

Billington, S. L. and Yoon, J., "Cyclic response of unbonded posttensioned precast columns with ductile fiber-reinforced concrete." *Journal of Bridge Engineering*, Vol 9, Issue 4, July 2004, pp. 353-363.

Fischer, G., and Li, V. C., "Deformation behavior of fiber-reinforced polymer reinforced engineered cementitious composite (ECC) flexural members under reversed cyclic loading conditions." *ACI Structural Journal*, Vol. 100, No. 1, January 2003, pp. 25-35.

Graybeal, B., "Material Property Characterization of Ultra-High Performance Concrete," FHWA, U.S. Department of Transportation, Report No. FHWA-HRT-06-103, McLean, VA, 2006

- Han, T.-S., Feenstra, P. H., and Billington, S. L., "Simulation of highly ductile fiber-reinforced cement-based composite components under cyclic loading." *ACI Structural Journal*, Vol. 100, No. 6, November 2003, pp. 749-757.
- Hosinieh, M. M., Aoude, H., Cook, W. D., and Mitchell, D., "Behavior of ultra-high performance fiber reinforced concrete columns under pure axial loading," *Engineering Structures*, Vol. 99, September 2015, pp. 388-401.
- Ibarra, L., and Bishaw, B., "High-Strength Fiber-Reinforced Concrete Beam-Columns with High-Strength Steel," *ACI Structural Journal*, Vol. 113, No. 1, January 2016, pp.147.
- Kawashima, K., Zafra, R., Sasaki, T., Kajiwara, K., and Nakayama, M., "Effect of polypropylene fiber reinforced cement composite and steel fiber reinforced concrete for enhancing the seismic performance of bridge columns," *Journal of Earthquake Engineering*, Vol. 15, No. 8, December 2011, pp. 1194-1211.
- Lafarge Canada Inc. " <https://www.lafarge.ca/en/ductal>., 2018.
- Legeron, F., and Paultre, P., "Uniaxial confinement model for normal-and high-strength concrete columns," *Journal of Structural Engineering*, Vol. 129, No. 2, February 2003, pp. 241-252.
- Mander, J. B., "Seismic design of bridge piers," University of Canterbury, Christchurch N.Z., 1984
- Mander, J. B., Priestley, M. J., and Park, R., "Theoretical stress-strain model for confined concrete." *Journal of structural engineering*, Vol. 114, No. 8, August 1988, pp. 1804-1826.
- Osorio, L. I., Paultre, P., Eid, R., and Proulx, J., "Seismic behavior of synthetic fiber-reinforced circular columns," *ACI Structural Journal*, Vol. 111, No. 1, January 2014, p. 189.
- Paultre, P., Legeron, F., and Mongeau, D., "Influence of concrete strength and transverse reinforcement yield strength on behavior of high-strength concrete columns," *Structural Journal*, Vol. 98, No. 4, July 2001, pp. 490-501.
- Popovics, S., "A numerical approach to the complete stress-strain curve of concrete," *Cement and concrete research*, Vol. 3, No. 5, September 1973, pp. 583-599.
- Razvi, S., and Saatcioglu, M., "Confinement model for high-strength concrete." *Journal of Structural Engineering*, Vol. 125, No. 3, March 1999, pp. 281-289.
- Sugano, S., Kimura, H., and Shirai, K. (2007). "Study of New RC Structures Using Ultra-High-Strength Fiber-Reinforced Concrete (UFC)," *Journal of advanced concrete technology*, Vol. 5, No. 2, 2007, pp. 133-147.

- Xu, S.-L., and Cai, X.-R., "Experimental study and theoretical models on compressive properties of ultrahigh toughness cementitious composites," *Journal of Materials in Civil Engineering*, Vol. 22, Issue 10, October 2010, pp. 1067-1077.
- Yang, C., and Okumus, P., "Ultrahigh-Performance Concrete for Posttensioned Precast Bridge Piers for Seismic Resilience," *Journal of Structural Engineering*, Vol. 143, No. 12, December 2017, p. 04017161.
- Zhang, Y.-y., Harries, K. A., and Yuan, W.-C., "Experimental and numerical investigation of the seismic performance of hollow rectangular bridge piers constructed with and without steel fiber reinforced concrete," *Engineering Structures*, Vol. 48, March 2013, pp. 255-265.
- Zhou, J., Pan, J., and Leung, C. K. (2014). "Mechanical behavior of fiber-reinforced engineered cementitious composites in uniaxial compression." *Journal of materials in civil engineering*, Vol. 27, No. 1, p. 04014111.

7. Acknowledgements

This research was supported by the Institute of Bridge Engineering, and the Department of Civil, Structural and Environmental Engineering at University at Buffalo, the State University of New York. LafargeHolcim and MMFX have generously donated materials for testing. The results, conclusions and opinions belong to the authors and do not necessarily reflect the views of the funding agencies and the parties acknowledged.